Journal of Materials Chemistry C

Unusual magnetic ordering transitions in nanoscale biphasic LuFeO3: Role of ortho-hexa phase ratio and local structure

Journal:	*Journal of Materials Chemistry C*
Manuscript ID	TC-ART-06-2020-002991.R1
Article Type:	Paper
Date Submitted by the Author:	26-Sep-2020
Complete List of Authors:	Chaturvedi, Smita; Interdisciplinary School of Science, savitribai Phule Pune University Pune India, Physics Shyam, Priyank; Indian Institute of Science Education and Research, Pune, Physics Shirolkar, Mandar; Symbiosis Center for Nanoscience and Nanotechnology Symbiosis International (Deemed University), Symbiosis Center for Nanoscience and Nanotechnology Krishna, Swathi; Indian Institute of Science Education and Research, Physics Sinha, Bhavesh; bKorea Institute of Materials Science, Materials Science Caliebe, Wolfgang; Deutsches Elektronen-Synchrotron, FS-PEX Kalinko, Aleksandr; University of Paderborn Departement of Chemistry Srinivasan, Gopalan; Oakland University, Ogale, Satishchandra; IISER Pune

ARTICLE

Unusual magnetic ordering transitions in nanoscale biphasic $LuFeO_3$: Role of ortho-hexa phase ratio and local structure

Received 00th January 20xx,
Accepted 00th January 20xx

DOI: 10.1039/x0xx00000x

Smita Chaturvedi, [a,b,i†] Priyank Shyam,[c] Mandar M. Shirolkar,[d,e,] Swathi Krishna[b], Bhavesh Sinha,[f] Wolfgang Caliebe,[g] Aleksandr Kalinko,[h] Gopalan Srinivasan [i] and Satishchandra Ogale[b,j†]

The Understanding nanoscale ferromagnetism is becoming increasingly important in view of our enhanced ability to control growth and morphological features of complex nano-systems and their potential translation into emergent high density magnetic device technologies. In this work, we have examined the combined consequences of the magneto-crystalline anisotropy, shape anisotropy, intrinsic phase coexistence, and surface induced self-strain and related anisotropy on the magnetism and magnetic transitions in the case of nanoparticles (NPs) and nanofibers (NFs) of the intriguing multiferroic $LuFeO_3$. We find that the two systems exhibit remarkable differences in the magnetic transitions as well as the value of the canted antiferromagnetic moment by virtue of significant differences in the relative hexagonal (h) and orthorhombic (o) phase content with h:o phase contribution in NPs (NFs) being 25:75 (77:23). In the case of NFs with major hexagonal component, the bifurcation of ZFC and FC magnetization curves is seen to occur above room temperature with a transition seen at about 150 K, a feature reflecting in-plane (a-b) antiferromagnetic order. In the case of NPs with dominant o-phase, a weak ferromagnetic (canted antiferromagnetic) signal is noted from 400 K (maximum measurement temperature) down to about 274 K, at which point antiferromagnetic susceptibility feature is seen. Below 223 K a reentrant ferromagnetic order is seen down to 153 K, at which point a bifurcation is noted between FC and ZFC curves. After subtracting the major component of the field dependent linear moment, the weak ferromagnetic(canted) moment at 300 K is almost 2 orders higher in the case of NFs than NPs. Detailed analysis of phase constitution, local structure and lattice-distortions is performed by x-ray diffraction, Raman spectroscopy, and synchrotron-based x-ray absorption near edge structure (XANES) spectroscopy. The potential significance of the interfaces in influencing the canting via gradient spin order distribution is emphasized.

1. Introduction

Ferroic order in materials and related phenomena have always attracted great interest among scientists and technologists alike. These primarily include ferromagnetism, ferroelectricity, piezoelectricity, and more recently multiferroicity. The order parameters involved in these phenomena are highly sensitive to various aspects of the materials properties and form via coupling with lattice-structure related parameters (e.g. magneto-crystalline anisotropy, strain, surfaces, interfaces, defects, dopants) and their relaxations in the case of composites, supported films and nanostructures. Numerous studies have been performed on various types and forms of such ferroic materials in the interest of applications in the domains of spintronics, memories (e.g. MRAM, FRAM), quantum computing etc.[1–3]

With the emergence and rapid growth of the field of nanotechnology and related processing technologies, it has now become possible to generate ordered arrays of nanostructures as device platforms for futuristic low energy consuming devices. These are envisioned as necessary vehicles for the emergent fields such as internet of things (IoT). It is, thus, of great interest to understand magnetism at nanoscale in systems of different shapes and forms. It is to be concurrently recognized that these forms can potentially display novel effects, which are different from the properties seen in the

[a]*Interdisciplinary School of Science, Savitribai Phule Pune University, Ganeshkhind , Pune - 411007, India*
[b]*Centre for Energy Science, Indian Institute of Science Education and Research, Pune - 411008, India*
[c]*Interdisciplinary Nanoscience Center, Aarhus University, Gustav Wieds Vej 14, Aarhus, Denmark*
[d]*Department of Physics, Tamkang University, Tamsui 251, Taiwan*
[e] *Symbiosis Centre for Nanoscience and Nanotechnology (SCNN), Symbiosis International (Deemed University), Lavale, Pune, 412115 India*
[f]*National Center for Nanosciences and Nantechnology, University of Mumbai,Kalina, Santakruz(E) Mumbai- 400098*
[g] *Deutsches Elektronen-Synchrotron, Photon Science, Notkestr, 85, 22607 Hamburg, Germany.*
[h]*Paderborn University, Warburger Strasse 100, 33098 Paderborn, Germany*
[i]*Physics Department, Oakland University, Rochester, Michigan 48309-4401*
[j] *Research Institute for Sustainable Energy, TCG-Centres for Research and Education in Science and Technology, Sector V, Salt Lake, Kolkata-700091, India*

† *Corresponding Author Email:*
smita.chaturvedi24@gmail.com
satish.ogale@tcgcrest.org, satishogale@iiserpune.ac.in

Electronic Supplementary Information (ESI) available:]. See
DOI: 10.1039/x0xx00000x

conventional bulk or thin film forms. In unsupported nano-systems, an interesting new feature is the surface-induced self-generated strain gradient (unlike the substrate-induced strain in supported films) which manifests itself differently in different shapes and forms of nanomaterials and can dramatically influence the phase equilibria as well. This is particularly true and important in materials where structural phase forms are not separated by large free energy differences. Since in the case of multiferroics the order parameters of two distinct ferroic orders are coupled, the nanoscale form factors could have dramatic influence on the emergent phenomena and properties.[4]

Another key factor which potentially brings out uncommon application-worthy behaviours in functional materials is the interface, since it has a crucial role in controlling and unveiling the interesting functionalities of materials. Indeed, a wide range of physical phenomena such as magnetism, ferroelectricity, multiferroicity, superconductivity and magnetoelectricity have their origin and control at interfaces via epitaxy, strain, reconstruction, polarity, dynamics of spins and orbitals, and electronic band alignments.[5–7] Interfaces between two distinct structural phases of the same material are even more exciting. Indeed, our recent study on $LuFeO_3$ brought out that the ferroelectric properties of nanoparticle and nanowire forms differ significantly due to dual phase coexistence, and as such support differing property-strengths in the application context.[8] Here, we show that the magnetic properties of nanoscale multiferroic $LuFeO_3$ also show equally exciting shape form-factor dependent property differences, that can be ascribed to the dual phase character and differing relative phase content of the two nano-systems. Coexisting phases also bring in the interesting aspect of the interface between the two, which could be clearly relevant and important for the emergent applications. Song et al. have reported that hexagonal-orthorhombic morphotropic phase mixture (MPM) realized in $LuFeO_3$ thin films concurrently exhibits ferroelectric polarization as well as weak ferromagnetic moment (WFM) as a consequence of the coupling across the interface between the h- and o-phases.[9] Cao et al. have examined the structural origin of single ion magnetic anisotropy in hexagonal and orthorhombic $LuFeO_3$ thin films by oxygen K-edge x-ray absorption spectroscopy (XAS) and found dramatic differences in the spectral features and linear dichroism. Based on the noted differences in the local environments of the Fe^{3+} and Lu^{3+} sites in the hexagonal and orthorhombic structures they have argued that the single ion anisotropy at the Fe^{3+} sites in $LuFeO_3$ originates from these uneven occupancies of the spin minority states via spin–orbit coupling.[10] Clearly, the coexistence of the two phases in a single material can be expected to show interesting consequences for magnetism in such a system; $LuFeO_3$ being a system with such potential.

$LuFeO_3$ is an oxide material with emerging interest in the intensely investigated field of multiferroicity. This is an extraordinary material, which exhibits both orthorhombic (o) and hexagonal (h) structures.[8–10] There is significant difference in lattice symmetry and coordination of Fe ion in the case of these o and h structures. $LuFeO_3$ has been explored by many groups in its hexagonal ceramic and thin film forms[11–17] and in the orthorhombic form.[18–21] Xu and coworkers studied the crystal and magnetic structures of h-$LuFeO_3$ (h-$LuFeO_3$: polar *P63cm* space group) and noted that the polar structure of the film persists at a high temperature of 1050 K, with indication of ferroelectricity based on room temperature switchability of the polar behavior. An antiferromagnetic (AFM) order was found below 440 K and a weak ferromagnetic order below 130 K emanating from spin reorientation.[11] Subsequently, Ratcliff and coworkers grew nominally similar films of h-$LuFeO_3$ on (0001) sapphire by molecular beam epitaxy and showed that the system orders into a ferromagnetically canted antiferromagnetic state via a single transition below 155 K regardless of film thickness[16], in contrast to the previous work by Wang et al. Later, Kumar et al. successfully stabilized single phase hexagonal $LuFeO_3$ in the bulk form without any doping by sol-gel method.[15] Multiple techniques were used to confirm the onset of antiferromagnetic order below 130 K. A clear anomaly was also seen in the dielectric data at $\sim T_N$ revealing the presence of magnetoelectric coupling.[11] A change was also noted in the lattice constants at T_N, implying a strong magnetoelastic coupling in the system. Masuno et al. stabilized the h-$LuFeO_3$ phase in bulk by Sc doping and the magnetic characterizations on bulk $Lu_{1-x}Sc_xFeO_3$ revealed a magnetic anomaly (probable antiferromagnetic ordering) at ~ 425-445 K, followed by magnetic transitions around ~167-172 K.[22] Clearly, there are differences in the reports on magnetic ordering and the corresponding temperatures depending on the form factor and strain state (substrate or dopant induced strain).

Hexagonal rare earth ferrites (h-$RFeO_3$) have antiferromagnetic spin structure due to structural symmetry leading to presence of triangularly-coupled Fe moments.[11,23–26] In such systems including h-$LuFeO_3$ the magnetic ordering temperature depends upon strong interaction between Fe^{3+}- Fe^{3+}, large Fe-O interaction and the frustration created by the triangular spin lattice. The frustration tends to lower the long range spin ordering temperature and the magnetic anisotropy energy.[27] The magnetic anisotropy energy in h-$LuFeO_3$ works against the frustration of the triangular lattice and contributes to the long range magnetic order, which in turn affects the magnetic transition temperature in the system.[25,26] This spin frustration due to local symmetry in h-$LuFeO_3$ introduces interesting magnetic phases. As reported by Cao et al., in o-$LuFeO_3$ the local environments of the Fe centres are the FeO_6 octahedra; hence no anisotropy can occur due to local symmetry at the Fe-site.[10] Conversely, in h-$LuFeO_3$, the local environment of the Fe centres are the FeO_5 trigonal bipyramids suggesting strong anisotropy between the a–b plane and the c axis due to local symmetry.

In this work we examine the consequences of the co-existence of significantly differing proportions of o-$LuFeO_3$ (o-LFO) and h-$LuFeO_3$ (h-LFO) phases introduced synthetically in two distinct nanoscale morphologies i.e. nanoparticles (NPs) and nanofibers (NFs) on the corresponding magnetic behavior. Our results show that significant differences are indeed seen in the magnetic transitions and canted antiferromagnetic moments in the two cases. Notably, the high density of internal biphasic

interfaces in nanosystems does provide the basis for defining the differences in coupling of the magnetic phases.[28,29]

2. Experimental

LFO-NP were synthesized using a sol-gel route combined with post-synthesis annealing.[30] For the synthesis of LFO-NF electrospinning technique was used as described previously.[8] The NPs and NFs were annealed up to temperatures just below the temperature of forming the pure orthorhombic phase, to assess the stability of hexagonal phase in different morphologies. In addition to different standard material characterizations, the investigation of local structure around the transition metal ion (Fe^{3+}) was performed by the X-ray Absorption Near Edge Structure (XANES) spectroscopy which reveals the variation of the local structure as the symmetry of the Fe ion changes. This information is key to the magnetic behaviour, since it directly impacts the dynamics of 3d-4p orbitals and crystal field splitting energy. Detailed experimental and characterization specifications are provided in the Electronic Supplementary Information (ESI).

3. Morphology and Phase determination

Figs. 1 (a1-i1) and (a2-i2) show the TEM, HRTEM images (showing the presence of orthorhombic and hexagonal phases), SAED pattern, and elemental mapping in STEM mode for NPs and NFs, respectively. The growth of *Pnma* and *P63cm* phases of LFO-NPs and NFs takes place in a manner such that, the *P63cm* phase nucleates first and the *Pnma* phase follows by

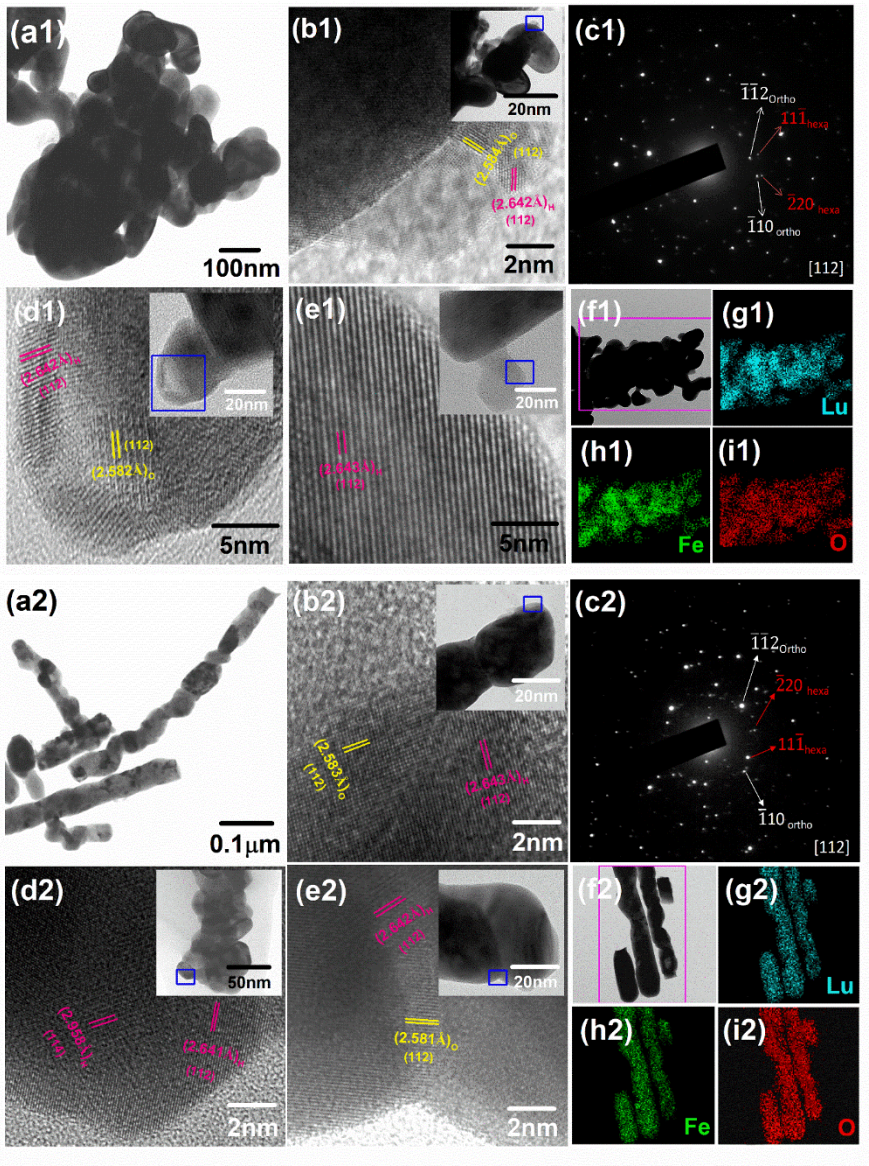

Figure 1. (a1, a2) TEM images, (b1,b2),(d1,d2) and (e1,e2) HRTEM showing presence of orthorhombic and hexagonal phases, (c1,c2) SAED and (f1,f2)-(i1,i2) mapping in STEM mode respectively for NPs and NFs.

strain relaxation.[8] Annealing to higher temperatures makes the material attain the *Pnma* phase.

We also observed that with the change in morphology from NPs to NFs, the *Pnma* phase undergoes an increase in strain while the *P63cm* unit cell slightly relaxes.[8] This shows that the growth mode for individual cases of NPs and NFs is quite different from that of the thin film growth model.[9]
Based on the observed angles between the (112) planes of the hexagonal and orthorhombic phases in the TEM images, the two phases are seen to be interfaced at ϕ such that 90°< ϕ<120°. The (112) plane is the one with maximal atomic density (and therefore, highest intensity in the *Pnma* phase's XRD profile) and near maximal atomic density (not an actual peak in the *P63cm* phase's XRD profile). This plane could form an interface between the two when rotated by a suitable non-trivial angle.[9]

4. XRD and Raman Spectroscopy: Confirmation of phase constitution

As presented in Table 1, the refinement of XRD data provides the calculated ratios of orthorhombic and hexagonal phases, the Fe-O-Fe angle, and the interatomic distances of Fe-O, for FeO_6 and FeO_5 polyheadra in case of NPs and NFs.[8] NFs have smaller Fe-O-Fe bond lengths than NPs. (X ray diffraction data are shown in Fig. S1 in ESI)

The intensity normalized Raman spectra for both the samples are shown in Fig. 2. The synthesis conditions and ionic radii of rare earth cation govern the phase of rare earth oxides.[31] According to group theory, the o-LFO phase exhibits $7A_g+5B_g+7B_{2g}+5B_{3g}$ Raman active modes, while the h-LFO phase shows $9A_1+14E_1+15E_2$ Raman active modes.[15,16,32] Table 2 shows the observed Raman modes and their attributes for both the cases observed over the scanning range of 100 to 700 cm^{-1}. The Raman peak positions for both the samples are in good agreement with the orthorhombic and hexagonal phases of $LuFeO_3$.[15,16,32]

Fig. 2 shows that in the case of NPs, o phase is dominant and h phase appears to be minor, which is exactly opposite in the NFs case. The Raman mapping shown in Figs. 2(b) and (c) for certain modes is helpful to quantify the phase contribution in the nanostructures. The Raman mapping for both the cases confirms the phase distribution (as established by Rietveld refinement of the XRD data), and also reveals that both phases have a phase boundary.[33] Moreover, it indicates that experimental conditions are favourable for the h-LFO to grow on the o-LFO structure controlling their relative concentration in both the morphologies.[34] Since free energy of formation of o-LFO is lower than that of h-LFO, this favours the formation of hexagonal phase on the orthorhombic phase to cross the energy barrier over the sub-micrometre length scale.[8,33]
For rare earth ferrites, the Raman modes below 200 cm^{-1} mainly describe the displacements of rare earth ions, while, motions of iron and oxygen ions are accounted for by the modes above 300 cm^{-1} [16,31,35,36] Thus, changes in the Lu - O and Fe - O bond lengths and FeO_5 bipyramidal tilt ultimately lead to shifts in the Raman modes.

.

Table 1. Critical structural parameters obtained Rietveld refinement of the X ray diffraction data[8]

					Pnma (o-Phase- FeO_6)				
	a	b	c	V	%	Fe-O	FeO_6	<Fe-O-Fe>	φ
NPs	5.55	7.56	5.21	218.54	75	2.99	10.71	144.847	17.58
NFs	5.56	7.57	5.22	219.36	23	3.04	10.79	144.327	17.84
					P63cm (h- phase- FeO_5)				
	a	b	c	V	%	Fe-O	FeO_5	<Fe-O-Fe>	φ
NPs	5.93	5.93	11.77	358.53	25	3.26	7.26	118.932	30.53
NFs	5.95	5.95	11.73	359.50	77	3.3	6.55	117.303	31.30

Table 2. Observed Raman modes in the present study and their one to one comparison with the reported Raman modes for orthorhombic and hexagonal phases, along with their designation

110	**110**	**-**	R-Motion	**110**	**-**	**E2**	+x,y(Fe,O3,O4) -x,y(Lu1,Lu2)	**115** (h)	**114** (h)
136	136	$A_g(6)$	**R-Motion**	-	135	E2	**+x,y(Lu1) -x,y(Lu2)**	133 **(o)**	133 **(o)**
160	158	$B_{2g}(5)$	**R- Motion**	-	148	A1	**+z(Lu1) -z(Lu2)**	158 **(o)**	155 **(o)**
-	-			-	190	A1	**rot. x,y(FeO_5)**	-	-
-	-			214	215	E2	**+x,y(O2,Fe) -x,y(O1,O3)**	-	-
225		Ag(2)	**FeO_6-Rotation**	223	257	A1	**+z(Lu1,Lu2) -z(Fe)**	252 **(h)**	251 **(h)**
290	278	$B_{1g}(3)$	**FeO6-Rotation**	289	297	A1	**x(Fe), z(O3)**	286 **(h)**	284 **(h)**
349	350	$A_g(7)$	**R-O Vibration**	346	302	E2	**+z(O2) -z(O1), x,y(O4)**	346 **(o)**	347 **(o)**
-	-			-	376	E1	**+x,y(O1) -x,y(O2)**	-	-
409	425		**R-O vibration**	404	408	E1	**+x,y(O1) -x,y(O2)**	407 **(h)**	406 **(h)**
-	-			-	433	A1	**+z(O4,O3) -z(Fe)**	-	-
-	-			-	459	A1	**+x,y(O1,O2) -x,y(Fe)**	-	-
428	427	$A_g(4)$	**FeO_6 bending**	448	458(c)	E2	**+x,y(O4) -x,y(O1,Fe)**	-	-
453	450	$B_{1g}(4)$	**FeO_6 bending**	473	-	A1		477 **(h)**	475 **(h)**
517	516			501	515(c)	E2	**+x,y(O4,O3) +x,y(O1,O2)**	516 **(o)**	514 **(o)**
608	-	$A_g(3)$	**FeO_6 stretching**	603	632	E1	**x,y(O3) -x,y(O4)**	-	-
644	654	$B_{2g}(2)$	**FeO_6 stretching**	651	681	A1	**+z(O1) -z(O2)**	644 **(h)**	646 **(h)**
-	-	$A_g(1)$	**FeO_6 stretching**	721	-	A1		-	-

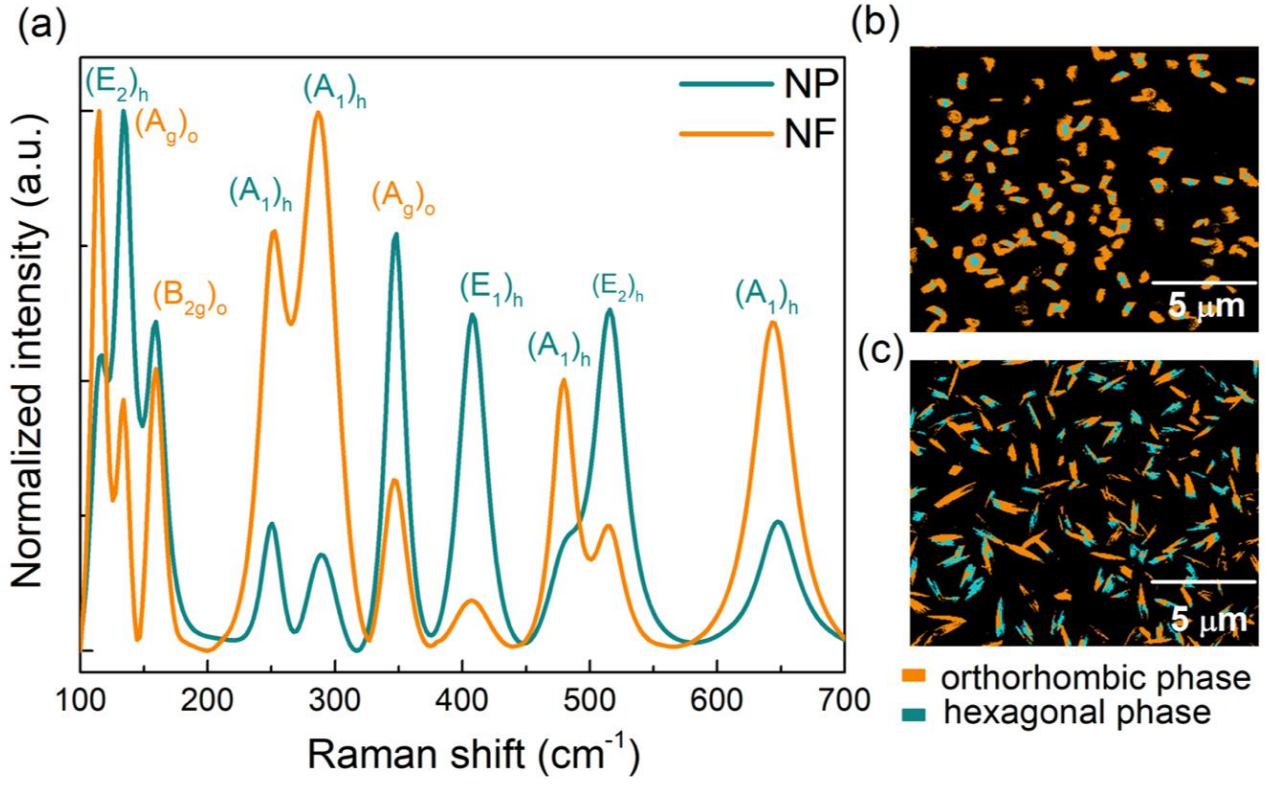

Figure 2. Raman spectroscopy study of LFO NPs and NFs. (a) normalized Raman spectra for both the cases. The highlighted region of both spectra shows Raman modes considered for Raman mapping, (b) and (c) show Raman mapping image obtained on selected Raman modes for NPs and NFs cases respectively.

5. Magnetic ordering and transitions

Figs. 3 (a) and (c) show the results of the temperature dependent magnetization measurement from room temperature down to 2 K for the NPs and NFs, respectively, for zero field cooled and field cooled cases. Remarkable differences are noted in the nature of the magnetization curves. The corresponding ferromagnetic contributions for the NFs and NPs cases after subtraction of the paramagnetic contributions (Raw data in ESI) are shown in Figs. 3 (b) and (d) respectively, and these show quite significant differences between the two cases. Magnetism in nanosystems is difficult to analyze for the case of canted ferromagnetism (anti-ferromagnetism with spin canting), when we have a biphasic system with strain gradients that are related to the shape. In the case of electrospun fibers, the strains are precipitated in the growth and natural directional sintering process. These strain gradients compounded with magneto-crystalline anisotropy and magneto-strictive effects make the situation rather complex. Given small value of magnetization, the demagnetization contributions corresponding to the two shapes is expected to be very small. As may be noted from the raw data shown in the supporting information (Figure S2), the magnetization studies covered a field range of -9 to +9 Tesla. A major paramagnetic component is noted, with the magnetization rising with the applied field. This rising component was subtracted to get the loops that are presented in Figs. 3 (b) and (d) of the main paper for comparison. Thus, the origin of apparent minor loop like features are not due to low field used in the measurement. Also, it is worth mentioning here that, the subtraction could potentially remove the AFM contribution. The major intent here is to establish the distinct qualitative (and to a limited extent quantitative) differences noted between the behaviors of Nanoparticles and Nanofibers.

In the case of NFs, which have the hexagonal phase as the major component, the bifurcation of ZFC and FC magnetization curves is seen to occur above room temperature and, at about 150 K, a feature reflecting in-plane (a-b) antiferromagnetic order, and concurrently an out-of-plane (c) weak ferromagnetism (canted antiferromagnetism) is observed – consistent with a previous report by Disseler et al.[16] Importantly, the value of the ferromagnetic saturation moment measured at room temperature is almost 44 x10^{-4} μ_B/Fe (0.09 emu/g), which cannot emanate from considering only the ortho-component (a minority phase in these NF samples) and known to only support weak ferromagnetic ordering.

It may be noted that these values of moments cannot be directly correlated with the values for epitaxial thin films or other idealized systems where the magnetization field direction can be suitably specified. For instance, in the work of Disseler et al.[16] the external field was specifically applied along the c-direction of the h-phase.

From the inset of Fig. 3(a) it may be noted that although the primary phase in the NFs is the h-phase, the magnetic signature of the minority phase (o-phase) does exist therein with weak ferromagnetic ordering at 617 K, with another weaker transition seen at as high a temperature as 835 K. A logical

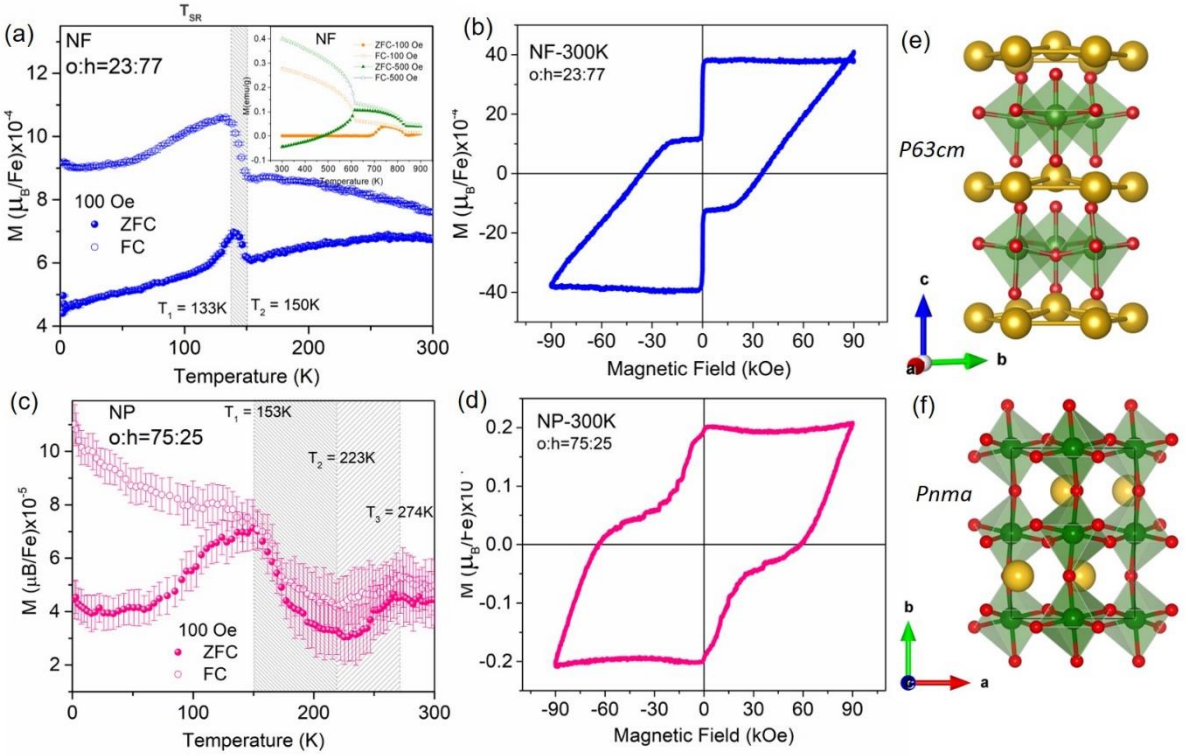

Figure 3. (a) and (c) Temperature dependent magnetization for temperature range 300 K to down 0 K for NFs and NPs respectively (error bars Included), (b) and (d) Ferromagnetic component (after paramagnetic/diamagnetic background removed) of MH hysteresis loop for NF and NP for 300 K and (e) and (f) hexagonal lattice and orthorhombic lattice schematic. Inset of (a) shows temperature dependent magnetization for temperature range 900 K to down 300 K for NFs.

consideration would suggest that the c axis of the h-phase would run along the NFs axis and as such the o-phase would form a shell around this phase, as shown in Scheme 1 in the ESI. It could be reasonably hypothesized that the FeO_6 octahedral tilts of the o-phase could transfer the strain into the outer layers of the core h-phase and cause substantially greater canting of the spins, thereby rendering a stronger saturation moment. This could lead to the development of a gradient spin order which evolves in a non-trivial manner. In fact, the room-temperature hysteresis loops in Fig. 3(b) show that upon reducing the applied magnetic field, one component of the spin order reverses at zero field (like superparamagnetic relaxation) and another component can only be reversed at very high coercive field. The corresponding nature is almost linear drop of the moment with increasing reverse magnetic field. The latter is perhaps commensurate with the suggested gradient-type spin ordering. In the case of NPs, the magnetic transitions show further unique and unreported features. With dominance of o-phase, one notices weak ferromagnetic signal (canted AFM) from 400 K (max measurement temperature) down to about 274 K, at which point antiferromagnetic susceptibility feature is seen. The magnetization is unmistakably seen to start dropping (clearly in the ZFC data, although not as strongly in the FC data) from 274K down to about 223 K, at which point it picks up again. The rise from 223K down to about 150K is also quite clear. These features are clearly seen in both, the FC and ZFC data. Below 223 K a re-entrant ferromagnetic order is seen which gains strength with lowering of the temperature down to 153 K, at which point a bifurcation is noted between FC and ZFC curves, signifying this to be the blocking temperature. It is intriguing that this temperature is quite close to the canted AFM ordering temperature reported by Disseler et al.[16] for the h-phase, possibly suggesting that the minority h-phase has a role to play in driving the unblocking of the spin order. Interestingly, for the NPs the saturation moment at 300 K after subtracting the paramagnetic contribution is only about 0.2 x $x10^{-4}$ μ_B/Fe (4 x 10^{-4} emu/g) as against 44x10^{-4} μ_B/Fe (9 x 10^{-2} emu/g), in case of NFs. Also, in this case, the drop in the magnetization after field reversal is gradual and not sharp as in the NFs, although the behavior of the two magnetic phases with two coercive fields is similar. Since for the NPs, the o-phase will strain-control the internal h-phase from all sides restricting the ease of spin canting, it is possible that weak ferromagnetic order does not develop completely. For NFs on the other hand, canting freedom is afforded along the c-axis, presumably directed along the axis of the fibers.

The observations and discussions presented above suggest that biphasic coexistence in the system at the nanoscale can lead to non-trivial magnetic behavior via the gradient strain and spin ordering driven by the interface. White has addressed the unique spin reorientation and spin ordering behaviors of a number of rare-earth orthoferrites. It is specifically shown that in the magnetic moment data the transitions do occur with finite span in temperature which in several cases are often substantial.

Further it is stated that spin reorientation can be substantially (as much as 100 K) influenced by thermal treatments. Such treatments can alleviate and modify the strain state and possibly disorders.[37] Indeed, doping in rare earth ferrites, which can induce or modify strains is also known to induce significant changes in the magnetic ordering temperatures. Cao et al. have discussed the structural origins of the single ion magnetic anisotropy in $LuFeO_3$ alongside addressing the interfacial aspect between coexisting phases. It is argued that for o-$LuFeO_3$, the predicted easy axis for the spins is the shortest axis (a axis) after the *D2h* distortion, while for h-$LuFeO_3$, the preferred spin orientations are in the intersection between the basal plane and the mirror plane of the C_S symmetry.[10] When the phases coexist, it has been shown that the inter-phase boundary has a tendency to align with the crystal planes of the h-$LuFeO_3$ phase. Seen in the context of the results presented here, it could actually provide a definitive setting for the strain state rather than a totally disordered random interface even in bulk or nanoscale samples.

Moreover, the magnetic ordering of Fe-O-Fe superexchange is sensitive to the bond angle and bond length.[38] The Fe-O-Fe superexchange angle is reduced in the case of NFs (Table1), which is also one of the factors favoring the enhanced magnetic moment. These observations and analysis are in coherence with the recent report by Suresh et al. wherein they have reported the coupling between lattice, electric and magnetic degrees of freedom in the case of bulk h-LFO based on neutron diffraction and X-ray diffraction.[39].

6. XANES: Confirming the role and significance of the local order and strains

In order to confirm the role and significance of the local order and strains in the observed magnetic behavior, we investigated the interaction between Lu and Fe sublattices in NPs and NFs using synchrotron XANES. Table 3 shows the calculated parameters.

The interplay between spin lattice frustration and magnetic anisotropy energy is a consequence of the local structure in the system around the Fe atom. Spin frustration in such system can present extraordinary magnetic phases.[40]

In the case of LFO NPs and NFs, we recorded the temperature dependent Fe K-edge XANES spectra. Fig. 4 (a) shows the pre edge and main-edge XANES spectra for NPs and NFs for temperature range 20 K to 300 K, measured at beamline P64 at PETRA III, DESY.[41] Fig. 4 (b) shows zoomed out view of pre-edge A and its splitting for NPs and NFs for various temperatures. Fig. 4 (c) shows the FeO_6 (FeO_5) polyheadra belonging to orthorhombic (hexagonal) phase symmetry. Since NFs dominantly have hexagonal phase, it exhibits non-centrosymmetry and lower coordination number of Fe. LFO NPs and NFs experience different amounts of distortion, owing to the difference in symmetry, morphology, and coordination of Fe atoms. This is observed experimentally, in terms of the difference in the signature of their pre-edge XANES spectra. The

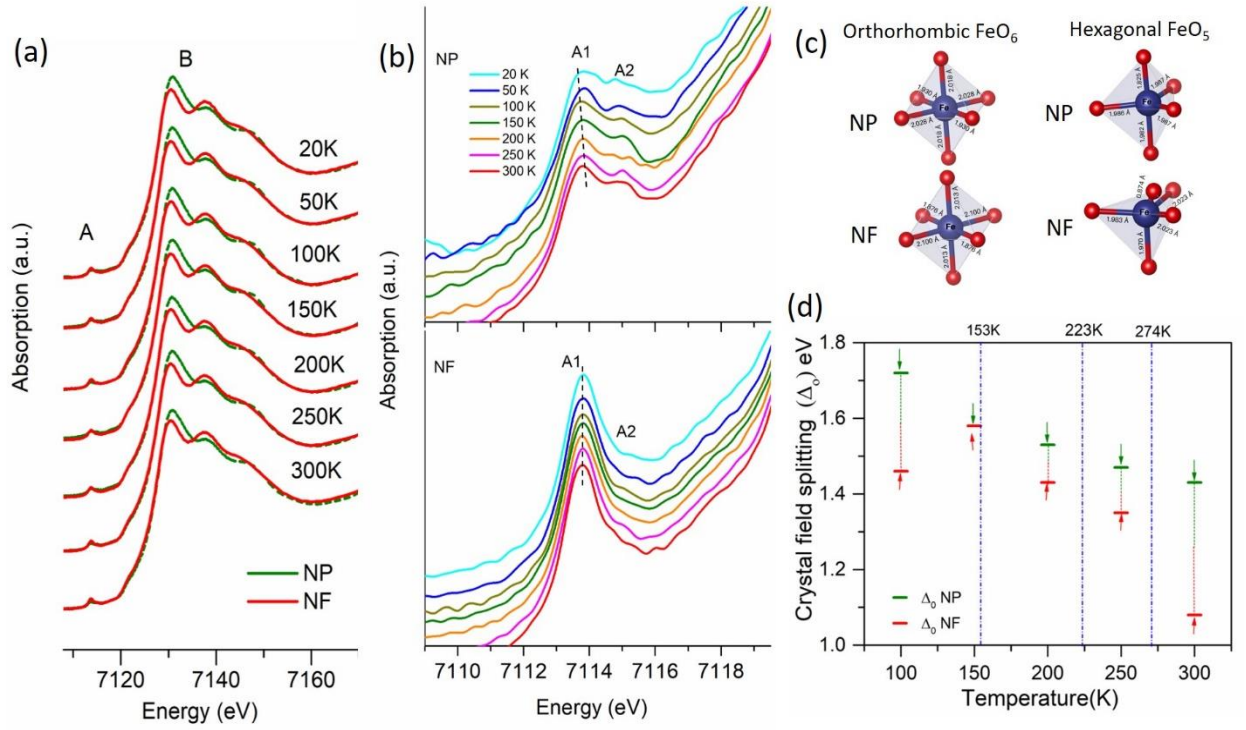

Figure 4. (a) Temperature dependent XANES Pre-edge (Peak A) and main peak for LFO-NPs and LFO-NFs, (b) splitting of pre-edge for temperatures 20,50,100,150,200, 250 and 300 K(dotted line for guide to eye) and (c) FeO_6 and FeO_5 polyheadra in case of orthorhombic and hexagonal phase respectively based on bond lengths calculated from Reitveld refinement of the XRD data. (d) the plot of calculated crystal field splitting against temperature.

decreased coordination number due to non-centrosymmetry (FeO_5) in NFs is confirmed by the higher intensity of pre-edge of NFs for all the temperatures as compared to that of NPs, which has dominant centrosymmetric attribute due to the presence of FeO_6 polyheadra in majority. Xu and coworkers examined the electronic structures for the conduction bands of both hexagonal and orthorhombic $LuFeO_3$ thin films by x-ray absorption spectroscopy at oxygen K (O K) edge and found dramatic differences in the spectral shape as well as the linear dichroism.[10] These differences were explained using the differences in crystal field splitting of the electronic states of the metals (Fe and Lu) and the differences in O 2p-Fe 3d and O 2p-Lu 5d hybridizations. The spectra were found to be sensitive to the changes in the local environments of the Fe^{3+} and Lu^{3+} sites in the hexagonal and orthorhombic structures (notably without change in the oxidation state

The crystal field splitting energy Δ_o of the d orbital of Fe atom is calculated using the absorption profile of pre-edge feature of the samples. The crystal field splitting energy values with their respective values of temperature for NPs and NFs are shown in Figure 4(d) and also in a table S1 in ESI . Lower value of Δ_o in the case of NFs as compared to that of NPs at 300 K can be attributed to the increase in the number of occupied states in the Fe 3d orbital in NFs. Hence, due to higher spin state, the hybridization of the O 2p and Fe 3d states is reduced and higher magnetization is observed. The three temperatures identified from Figure 3 (c) are indicated by blue dotted line. Interestingly, the crystal field splitting is seen to get reduced significantly in a temperature window across 274 K and it vanishes at about 153 K. The change across 223K does not appear as significant.

Conclusions

In summary, we have studied magnetism in nanoscale $LuFeO_3$ for two stoichiometric morphological forms, namely nanoparticles and nanofibers. The results reveal that the combined effects of the single ion magnetic anisotropy, shape anisotropy, intrinsic phase coexistence, and surface induced self-strain appear to render significant differences in the two cases. In the NFs the bifurcation of ZFC and FC curves is seen above room temperature with another transition at about 150 K, reflecting in-plane (a-b) antiferromagnetic order. On the other hand, in NPs a weak (canted) ferromagnetic signal is noted from 400 K (maximum measurement temperature) down to about 274 K, at which point an antiferromagnetic susceptibility feature is seen. Below 223 K, a reentrant stronger ferromagnetic order is seen down to 153 K, at which point a bifurcation is noted between FC and ZFC curves. After accounting for the major component of the field dependent linear moment, the weak ferromagnetic moment at 300 K is almost two orders higher in the case of NFs than NPs. Based on a detailed analysis of phase constitution, local structure, and lattice-distortions; the potential significance of the interfaces in controlling the magnetic ordering and the magnetic moment is emphasized.

Conflicts of interest

There are no conflicts to declare.

Acknowledgements

This work was carried out under the Grant No. SR/WOS-A/PM-16/2016 from the Department of Science and Technology, Ministry of Science and Technology, India, and a Fulbright Fellowship Grant No. 2372/F-N APE FLEX/2018 availed by S.C. The research at Oakland University was supported by grants (DMR-1808892; ECCS-1923732). The authors also acknowledge the TEM measurements facility provided by SAIF IIT Bombay India. We acknowledge DESY (Hamburg, Germany), a member of the Helmholtz association HGF, for the provision of experimental facilities. Parts of this research were carried out at PETRA III. SBO acknowledges funding support from DST Nanomission under the Thematic Unit program and the Department of Atomic Energy for the Raja Ramanna Fellowship award.

References

1 J. F. Scott, *Nat. Mater.*, 2007, **6**, 256–257.
2 N. A. Spaldin and R. Ramesh, *Nat. Mater.*, 2019, **18**, 203–212.
3 I. Maksymov, *Nanomaterials*, 2015, **5**, 577–613.
4 A. N. Morozovska, M. D. Glinchuk and E. A. Eliseev, *Phys. Rev. B - Condens. Matter Mater. Phys.*, 2007, **76**, 014102.
5 A. R. Akbashev, V. V. Roddatis, A. L. Vasiliev, S. Lopatin, V. A. Amelichev and A. R. Kaul, *Sci. Rep.*, 2012, **2**, 2–5.
6 R. Ramesh and D. G. Schlom, *Nat. Rev. Mater.*, 2019, **4**, 257–268.
7 R. Ramesh, *Curr. Sci.*, 2013, **105**, 1107–1114.
8 S. Chaturvedi, S. K. Singh, P. Shyam, M. M. Shirolkar, S. Krishna, R. Boomishankar and S. Ogale, *Nanoscale*, 2018, **10**, 21406–21413.
9 S. Song, H. Han, H. M. Jang, Y. T. Kim, N. Lee, C. G. Park, J. R. Kim, T. W. Noh and J. F. Scott, *Adv. Mater.*, 2016, **28**, 7430–7435.
10 S. Cao, X. Zhang, T. R. Paudel, K. Sinha, X. Wang, X. Jiang, W. Wang, S. Brutsche, J. Wang, P. J. Ryan, J. W. Kim, X. Cheng, E. Y. Tsymbal, P. A. Dowben and X. Xu, *J. Phys. Condens. Matter*, 2016, **28**, 156001.
11 W. Wang, J. Zhao, W. Wang, Z. Gai, N. Balke, M. Chi, H. N. Lee, W. Tian, L. Zhu, X. Cheng, D. J. Keavney, J. Yi, T. Z. Ward, P. C. Snijders, H. M. Christen, W. Wu, J. Shen and X. Xu, *Phys. Rev. Lett.*, 2013, **110**, 237601.
12 X. Xu and W. Wang, *Mod. Phys. Lett. B*, 2014, **28**, 1430008.
13 V. V. Roddatis, A. R. Akbashev, S. Lopatin and A. R. Kaul, *Appl. Phys. Lett.*, 2013, **103**, 1–6.
14 Y. K. Jeong, J. H. Lee, S. J. Ahn and H. M. Jang, *Chem. Mater.*, 2012, **24**, 2426–2428.
15 P. Suresh, K. V. Laxmi and P. S. A. Kumar, in *AIP Conf. Proc.*, 2016, vol. 1728, p. 020472.
16 S. M. Disseler, J. A. Borchers, C. M. Brooks, J. A. Mundy, J. A. Moyer, D. A. Hillsberry, E. L. Thies, D. Tenne, J. Heron, M. E. Holtz, J. D. Clarkson, G. M. Stiehl, P. Schiffer, D. A. Muller, D. G. Schlom and W. D. Ratcliff, *Phys. Rev. Lett.*, 2015, **114**, 217602.
17 W. Wang, H. Wang, X. Xu, L. Zhu, L. He, E. Wills, X. Cheng, D. J. Keavney, J. Shen, X. Wu and X. Xu, *Appl. Phys. Lett.*, 2012, **101**, 24907.
18 U. Chowdhury, S. Goswami, D. Bhattacharya, J. Ghosh, S. Basu and S. Neogi, *Appl. Phys. Lett.*, 2014, **105**, 052911.
19 M. Zhou, H. Yang, T. Xian, R. S. Li, H. M. Zhang and X. X. Wang, *J. Hazard. Mater.*, 2015, **289**, 149–157.
20 Y. Qin, X. Qiang Liu and X. Ming Chen, *J. Appl. Phys.*, 2013, **113**, 3–8.
21 T. Ahmad and I. H. Lone, *Mater. Chem. Phys.*, 2017, **202**, 50–55.
22 A. Masuno, A. Ishimoto, C. Moriyoshi, N. Hayashi and H. Kawaji, *Inorg. Chem.*, 2013, **52**, 11889.
23 S. A. Klimin, M. N. Popova, B. N. Mavrin, P. H. M. van Loosdrecht, L. E. Svistov, A. I. Smirnov, L. A. Prozorova, H.-A. K. von Nidda, Z. Seidov, A. Loidl, A. Y. Shapiro and L. N. Demianets, *Phys. Rev. B*, 2003, **68**, 174408.
24 S. Mitsuda, M. Mase, K. Prokes, H. Kitazawa and H. Aruga Katori, *J. Phys. Soc. Japan*, 2000, **69**, 3513–3516.
25 S. G. Condran and M. L. Plumer, *J. Phys. Condens. Matter*, 2010, **22**, 162201.
26 A. P. Ramirez, *Annu. Rev. Mater. Sci.*, 2003, **24**, 453–480.
27 H. Kirchmayr, eds. K. H. J. Buschow, R. W. Cahn, M. C. Flemings, B. Ilschner, E. J. Kramer, S. Mahajan and P. B. T.-E. of M. S. and T. Veyssière, Elsevier, Oxford, 2001, pp. 4754–4757.
28 S. Ramirez, K. Chan, R. Hernandez, E. Recinos, E. Hernandez, R. Salgado, A. G. Khitun, J. E. Garay and A. A. Balandin, *Mater. Des.*, 2017, **118**, 75–80.
29 B. Issa, I. M. Obaidat, B. A. Albiss and Y. Haik, *Int. J. Mol. Sci.*, 2013, **14**, 21266–21305.
30 S. Chaturvedi, P. Shyam, A. Apte, J. Kumar, A. Bhattacharyya, A. M. Awasthi and S. Kulkarni, *Phys. Rev. B*, 2016, **93**, 174117.
31 S. M. Feng, L. J. Wang, J. L. Zhu, F. Y. Li, R. C. Yu, C. Q. Jin, X. H. Wang and L. T. Li, *J. Appl. Phys.*, 2008, **103**, 026102.
32 S. Venugopalan and M. M. Becker, *J. Chem. Phys.*, 1990, **93**, 3833–3836.
33 S. Cao, X. Zhang, K. Sinha, W. Wang, J. Wang, P. A. Dowben and X. Xu, *Appl. Phys. Lett.*, 2016, **108**, 202903.
34 J. A. Moyer, R. Misra, J. A. Mundy, C. M. Brooks, J. T. Heron, D. A. Muller, D. G. Schlom and P. Schiffer, *APL Mater.*, 2014, **2**, 12106.
35 N. T. M. Hien, X. B. Chen, L. H. Hoang, D. Lee, S. Y. Jang, T. W. Nohc and I. S. Yanga, *J. Raman Spectrosc.*, 2010, **41**, 983–988.
36 M. Iliev, H. Lee and V. Popov, *Phys. Rev. B*, 1997, **56**, 2488–2494.
37 R. L. White, *J. Appl. Phys.*, 1969, **40**, 1061–1069.
38 C. S. Chen, C. S. Tu, P. Y. Chen, V. H. Schmidt, Z. R. Xu and Y. Ting, *J. Alloys Compd.*, 2016, **687**, 442–450.
39 P. Suresh, K. Vijaya Laxmi, A. K. Bera, S. M. Yusuf, B. L. Chittari, J. Jung and P. S. Anil Kumar, *Phys. Rev. B*, 2018, **97**, 184419.
40 A. Muñoz, J. A. Alonśo, M. J. Martínez-Lope, M. T. Casáis, J. L. Martínez and M. T. Fernández-Díaz, *Phys. Rev. B - Condens. Matter Mater. Phys.*, 2000, **62**, 9498–9510.
41 W. A. Caliebe, V. Murzin, A. Kalinko and M. Görlitz, *AIP Conf. Proc.*, 2019, **2054**, 60031.

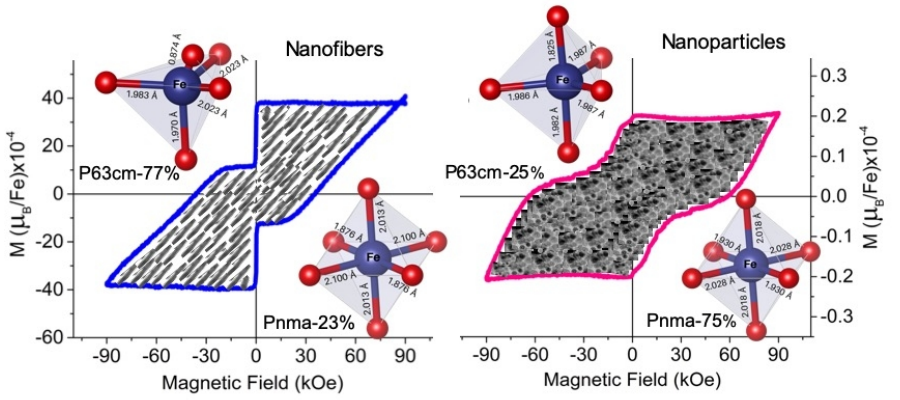

Significant differences in nanoscale magnetism of nanoparticle and nanofibre of biphasic $LuFeO_3$

340x168mm (72 x 72 DPI)